PCCP

Accepted Manuscript

ROYAL SOCIETY OF CHEMISTRY

www.rsc.org/pccp

Journal Name

ARTICLE

Received 00th January 20xx,

Accepted 00th January 20xx

DOI: 10.1039/x0xx00000x

www.rsc.org/

Molten Salts Medium Synthesis of Wormlike Platinum Silver Nanotube without any organic Surfactant or Solvent for Methanol and Formic Acid Oxidation

Haidong Zhao,[a] Rui Liu,[a] Yong Guo*[a] and Shengchun Yang*[b,c]

In current research, the Pt_xAg_y (x/y=86/14, 79/21, 52/48, 21/79, 11/89) nanoparticles (NPs) are synthesized in the KNO_3-$LiNO_3$ molten salts without using any organic surfactant or solvent. The SEM results suggest that when the content of Ag is higher than 48%, the wormlike Pt_xAg_y nanotubes (NTs) can be synthesized. The diameter of the Pt_xAg_yNTs shows a slow decrease with the increase of Ag content. The TEM and HRTEM results indicate that the growth of hollow Pt_xAg_y NTs undergo an oriented attachment process and a kirkendall effect approach. The results of cyclic voltammetry (CV) measurement indicates that the $Pt_{52}Ag_{48}$ catalyst presents a remarkable enhancement for methanol electrooxidation, while the $Pt_{86}Ag_{14}$ catalyst prefers electrochemically oxidizing the formic acid compared with that of the commercially available Pt black.

1. Introduction

Platinum-based alloy have attracted considerable attention in the fuel cell field and electrocatalytic application, due to their high catalytic activity and low cost[1-3]. As is well-known, the preparation methods and synthetic routes usually have a great influence on the catalytic activity of the bimetallic alloy NPs[4]. The platinum-based bimetallic alloy NPs, such as PtAg[5-7], PtCu[8-10], PtPb[11, 12], PtPd[13], PtRh[14], Pt_3Ni[15] etc., can be directly prepared by co-reduction of metal ions in aqueous or organic solution with the capping agents (e.g. CTAB/CTAC, PVP, oleylamine/oleic acid etc.,) presence [13, 15-17]. The capping agent layer (''stabilizer'') which covering on the surface of NPs will tremendously passivate the performance of the catalyst[18]. Therefore, the NPs must be cleaned by chemical, thermal and plasma approaches before it is used as the catalyst, but these treatments are not always effective[15]. Furthermore, the highly toxic organic surfactants and solvents, which are excessively used in the synthesis, will lead to complicating the preparation procedure, restricting their commercial applications, and causing serious environmental pollution. Hence, exploring facile, green, and capping agent/ organic solvent-free methods, which can be used to prepare platinum and platinum-based alloy NPs with clean surfaces, is still a challenge for the catalytic field.

In our previous research, we developed a green molten salts method, which have been proven to be a facile, effective and green approach for the synthesis of surfactant-free platinum and platinum-based alloy NPs[19-21]. For example, we successfully prepared the Pt nanosheets[19], Pt[20] and Pt_xCu_y[21] concave NPs in the molten salts of KOH-NaOH and KNO_3-$LiNO_3$ without using any capping agent or organic solvent. Notably, the Pt concave NPs prepared through this organic-free method are actually with very "clean" surface, as well as many high index facets and exposed atom steps, thus exhibiting an enhanced catalytic activity toward methanol oxidation compared with the commercial used Pt/C[20]. This approach offers a green and eco-friendly method to synthesize the platinum and platinum-based alloy NPs.

In current case, we demonstrate that the molten salts medium method can be successfully employed for the synthesis of wormlike Pt_xAg_y NTs, and their electrocatalytic activity toward methanol and formic acid electrooxidation are also investigated.

2. Experimental

2.1 Materials.

$LiNO_3$ (CR, 98.0%), silver acetate (CH_3COOAg, AR, 99.0%), tetra-ammine platinum oxalate ($Pt(NH_3)_4C_2O_4$, AR, 99.0%), methanol (CH_3OH, HPLC, 99.9%), formic acid (HCOOH, HPLC, 99.0%) and Pt black (JM) were purchased from Aladdin Reagent Company. KNO_3 (Tianjin Hengxing Chemical Reagent, AR, 99.0%), KOH

[a] School of Chemistry and Environmental Engineering, Shanxi Datong University, Datong 037009, Shan Xi, People's Republic of China. Email: ybsy_g@263.net (Y. G).

[b] School of Science, Key Laboratory of Shaanxi for Advanced Materials and Mesoscopic Physics, State Key Laboratory for Mechanical Behavior of Materials, Xi'an Jiaotong University, Xi'an 710049, Shaanxi, People's Republic of China.Email: ysch1209@mail.xjtu.edu.cn (S. Y), Fax, +86-29-82665995; Tel, +86-29-82663034

[c] Collaborative Innovation Center of Suzhou Nano Science and Technology, Xi'an 710049, Shaanxi, People's Republic of China.

Electronic Supplementary Information (ESI) available:. See DOI: 10.1039/x0xx00000x

(Tianjin Hengxing Chemical Reagent, AR, 85.0%), $HClO_4$ (Tianjin Xinyuan Chemical Reagent, GR, 70.0-72.0%), 2-propanol (Tianjin Fuyu Chemical Reagent, AR, 99.8%) and 5% Nafion solution (Aldrich Chemistry). All chemicals were used as received without further purification.

2.2 Preparation of the Pt_xAg_y alloy NPs.

The typical preparation procedure of the Pt_xAg_y NPs is as follows: 6.6 g of KNO_3 and 3.4 g of $LiNO_3$ were mixed and heated to 170 ^oC with magnetic stirring to form the molten salts (the eutectic temperature of $LiNO_3$ and KNO_3 is 125°C, Fig.S1), and kept the temperature until all the salts dissolved. Then, with vigorously stirring, the calculated amount of CH_3COOAg, $Pt(NH_3)_4C_2O_4$ and 22.4 mg KOH were added into the glass flask. The reaction was keep stirring in air for 2 h at 170^oC, and then naturally cooled down to room temperature. Then, the products were washed 3 times with distilled water to remove the residual salts. For the preparation of wormlike Pt_xAg_y NTs, the content of Ag should be higher than 48% in the precursors (seeing supporting information for details).

2.3 Characterization Methods.

The Powder X-ray diffraction (XRD) patterns of the Pt_xAg_yNPs were measured on a Bruker D8 advance X-ray diffractometer. The scanning electron microscope (SEM) images characterized on a JEOL 7000F field emission SEM system, and the average atomic compositions of the Pt_xAg_y NPs were obtained by the energy-dispersive X-ray (EDX) integrated with the SEM system. The transmission electron microscopy (TEM) system of JEOL 3010 with 300 kV acceleration voltages was used to analyze the TEM and high-resolution TEM (HRTEM) images.

2.4 Electrochemical Measurements

The performance of the Pt_xAg_y NPs in acidic ($HClO_4$) media was carried out on an electrochemical workstation (Pine AFCBP1) by using CV technique. The reference and counter electrodes used the saturated calomel electrode (SCE) and a 1cm×1cm platinum plate (99.9%), respectively. The 0.1 M $HClO_4$, which diluted from the stock solution with distilled water, was used as electrolyte. The working electrode prepared by ultrasonically dispersing 5 mg of the Pt_xAg_y catalyst in 5 mL mixed solvent which contained distilled water, 2-propanol and 5% Nafion solution with the volume ratio of 4: 1: 0.025. A quantity of 10 μL of the dispersion was dropped onto the top of glassy carbon electrode and dried in air for obtaining the working electrode. The CV tests were carried out in nitrogen (99.9%)-saturated 0.1 M $HClO_4$ solution at room temperature with the scanning rate of 50 mV s^{-1} and in the potential region from 0.02 to 1.1 V. The activities of Pt_xAg_y alloy electrooxidation methanol were measured in 0.1 M $HClO_4$ + 1 M CH_3OH solution with a scanning rate of 50 mV s^{-1}. And that of Pt_xAg_y NPs electrocatalytic oxidation formic acid were measured in 0.1 M $HClO_4$ + 0.5 M HCOOH solution with a scanning rate of 100 mV s^{-1}. In all of the experiments, stable CV curves were recorded after 50 cycles.

3. Results and discussion

The typical SEM and enlarged SEM images of the as-prepared Pt_xAg_y alloy NPs with different feeding molar ratios of $Pt(NH_3)_4C_2O_4$/ CH_3COOAg 8:1, 4:1, 1:1, 1:4 and 1:8 were shown in Fig. 1. According to the EDX results (Table 1), the obtained products were named as $Pt_{86}Ag_{14}$, $Pt_{79}Ag_{21}$, $Pt_{52}Ag_{48}$, $Pt_{21}Ag_{79}$ and $Pt_{11}Ag_{89}$, respectively. The average atomic compositions of these NPs matched well with the feeding ratios of precursors. From Fig. 1a and 1b, we can see that the as-prepared $Pt_{86}Ag_{14}$ and $Pt_{79}Ag_{21}$ NPs have relatively uniform size and shape. With decreasing the content of the Pt, the average particle sizes show a slow decrease from 82.5±12.1 nm for $Pt_{86}Ag_{14}$ to 69.6±12.2 nm for $Pt_{79}Ag_{21}$ NPs, and to 59.4±11.5 nm for $Pt_{52}Ag_{48}$. (Fig. S1a-c). When the content of Ag was higher than 48%, the Pt_xAg_y NTs, as well as some NPs in the product can be observed. (Fig. 1c, d and e). And the SEM results also indicated that the proportions of NTs in the products prepared at higher Ag ratios are obviously higher than the samples obtained at lower Ag ratios. The diameter of these NTs shows a slow decrease from 32.1±5.9 nm for $Pt_{52}Ag_{48}$ to 20.9±4.6 nm for $Pt_{21}Ag_{79}$, and to 15.2±2.4 nm for $Pt_{11}Ag_{89}$. (Fig. S1 d-f) While in the reaction system when CH_3COOAg was use as the only precursor (the content of Ag was 100%), only irregular Ag NPs with the average particle sizes about 104.3±28.3 nm were obtained. (Fig. 1f and S1g)

The TEM images of the $Pt_{52}Ag_{48}$ were shown in Fig. 2. As one can see from the Fig. 2a, most of the particles show a hollow interior and a worm like morphology, indicating the formation of the wormlike Pt_xAg_y NTs. Fig. 2b and 2c are local area enlarged images of Fig. 2a. The wall thickness and diameter of the as-formed $Pt_{52}Ag_{48}$ NTs was about 7.1 nm and 27.8 nm, respectively. (Fig. 2b) From the insert image in Fig. 2b, the nanotube (NT) structure can be further identified. Fig. 2c

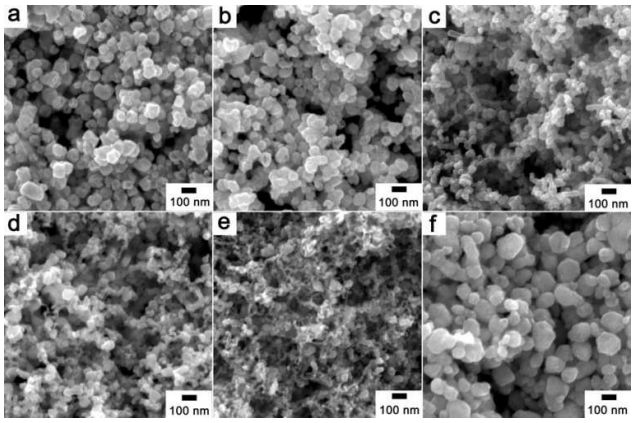

Fig. 1 SEM images of the (a) $Pt_{86}Ag_{14}$, (b) $Pt_{79}Ag_{21}$, (c) $Pt_{52}Ag_{48}$, (d) $Pt_{21}Ag_{79}$, (e) $Pt_{11}Ag_{89}$, (f) Ag.

Journal Name

ARTICLE

Table 1 EDX analysis of Pt_xAg_y atomic molar ratios in the alloy NPs prepared at different $Pt(NH_3)_4C_2O_4$ / CH_3COOAg feeding ratios.

Sample Pt_xAg_y	$Pt_{86}Ag_{14}$	$Pt_{79}Ag_{21}$	$Pt_{71}Ag_{29}$	$Pt_{52}Ag_{48}$	$Pt_{36}Ag_{64}$	$Pt_{21}Ag_{79}$	$Pt_{11}Ag_{89}$
As added molar ratio (x : y)	8:1	4:1	2:1	1:1	1:2	1:4	1:8
EDX value molar ratio (x : y)	6.1: 1.0	3.9:1.0	2.4:1.0	1.1:1.0	1.0:1.7	1.0:3.9	1.0: 8.5

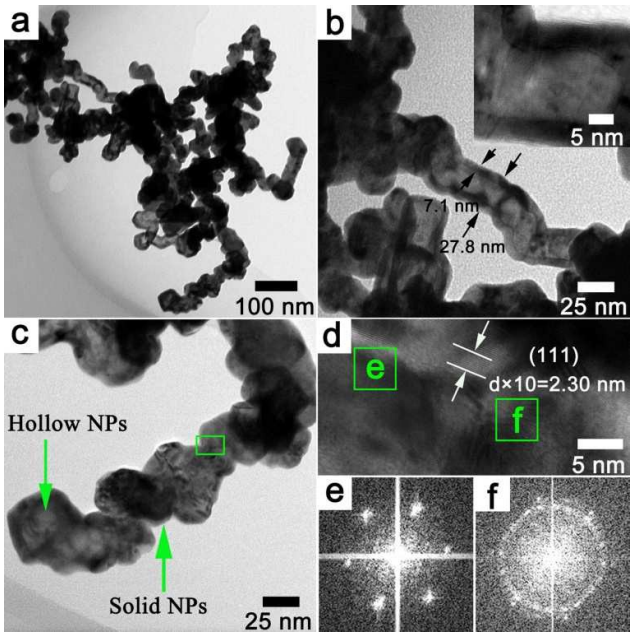

Fig. 2 (a), (b) and (c) TEM images of the $Pt_{52}Ag_{48}$; (b) and (c), the enlarged local area of (a); the inset image in (b) is the enlarge TEM images of the hollow nanotube; (d), HRTEM image of the $Pt_{52}Ag_{48}$ labeled with square in (c); (e), (f) FFT images of $Pt_{52}Ag_{48}$ labeled in (d).

shows the enlarged image of quasi NT aggregated with several NPs from which both of the NPs with and without hollow interiors can be observed as shown by the arrows in the image. Fig. 2d shows the HRTEM image of the $Pt_{52}Ag_{48}$ NTs labeled with a square in Fig. 2c. The fringe spacing (0.230 nm) fell in the range between those two pure monometal of the Pt and Ag, which can be defined to the (111) plane of the PtAg alloy[22], illustrating the PtAg alloy NTs are obtained. As shown in Fig. 2e, the discrete and hexagonal spots in the FFT pattern of a selected grain indicates a high degree of crystallinity of the alloy NPs. While the FFT pattern obtained from the grain boundaries (Fig. 2f) presents a circular point distribution, indicating a random distribution of lattice

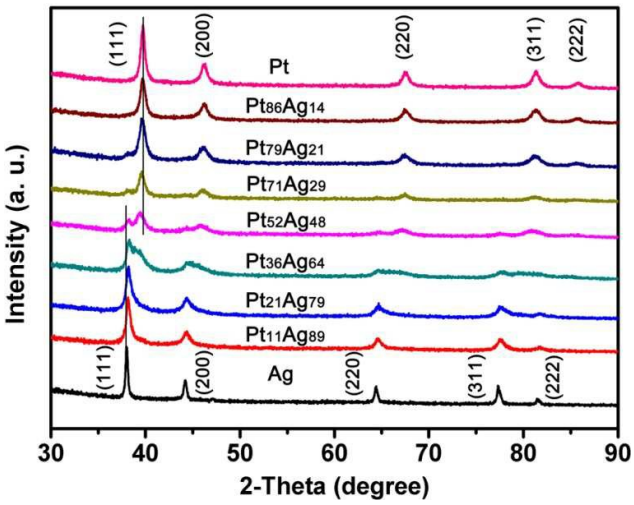

Fig. 3 XRD patterns of the Pt, $Pt_{86}Ag_{14}$, $Pt_{79}Ag_{21}$,$Pt_{71}Ag_{29}$,$Pt_{52}Ag_{48}$,$Pt_{36}Ag_{64}$, $Pt_{21}Ag_{79}$, $Pt_{11}Ag_{89}$, and Ag.

orientation of the attached grains. The growth process can be further revealed by the HRTEM characterizations as shown in Fig. S2. From Figs. S2a and S2d one can see that several septums obviously divides the hollow interiors, while a partially broken septum can also be observed as shown by the red arrow in Figs. S2a and S2b. These observations imply that the formation of wormlike NTs can be firstly due to the linear aggregation of NPs to form a wormlike nanowire, and then the Kirkendall effect induces the diffusion of two kinds of alloy element and form the hollow tubular structure[1, 23-25].

Fig. 3 shows the XRD patterns of Pt_xAg_y, pt and Ag NPs. As one can see that the diffraction peaks of the $Pt_{86}Ag_{14}$, $Pt_{21}Ag_{79}$ and $Pt_{11}Ag_{89}$ locating at the Pt-rich and Ag-rich region can be identified with the crystal planes of (111), (200), (220), (311), and (222), respectively, in response to a face-centered cubic (fcc) structure. The Pt_xAg_y NPs diffraction peaks located between the corresponding positions of pure metallic Pt and

Ag indicates that the alloy phase was obtained[25]. From the Fig. 3 we also can see that all diffraction peaks were shifted synchronously to lower angles with the decrease of pt proportion in the NPs. The redundant diffraction peak showed in the alloy of $Pt_{79}Ag_{21}$, $Pt_{71}Ag_{29}$, $Pt_{52}Ag_{48}$ and $Pt_{36}Ag_{64}$ can be due to the mixture of diffraction peaks from Pt-rich and Ag-rich region alloy. For pt-Ag bimetallic bulk materials, a large miscibility gap would exists when the temperature below about 1200 °C (Fig. S3). Therefore, the bulk PtAg alloy only could be formed at very high atomic compositions ratio of either Pt or Ag. For example, when the Pt and Ag elements atomic ratio falls outside the range between Ag_2Pt_{98} and $Ag_{95}Pt_5$ below 400 °C, the PtAg bulk materials would exist in two phases: one is Ag-rich and the other is Pt-rich alloys[26]. Yang Hong et. al. reported that the Pt-Ag alloy NPs (Pt/Ag molar ratio from 4/1 to 1/4) can be prepared in solution system from their corresponding precursors salts[25]. And similar with our current research, the XRD result in Fig. 3 is a powerful evidence for the obtained of Pt-Ag alloy in nanoscale.

In order to study the formation process of the Pt_xAg_y alloy NTs, the products obtained at different reaction time were analyzed through the SEM and EDX (Fig. 4). In the first 2 minutes, only a lot of irregular NPs can be observed, and the EDX results indicates that only Ag and Pt elements with the atomic ratio about 2.7:1 were detected except for basal Si signal. (Fig. 4a) The ratio of Ag in the product is far higher than that of Pt, which is mainly due to the CH_3COOAg thermal decomposition rate faster than that of the $Pt(NH_3)_4C_2O_4$, then the Ag-rich phase is generated. However, only after further 2 minutes, as shown in Fig. 4b, some irregular NPs aggregating into worm-like nanostructure can be found. The composition of pt dramatically increased with the atomic ratio about 1:1.3 for Ag and Pt elements, suggesting the Pt precursor was decomposed quickly after the first 2 minutes, and the large quantities of pt atoms adsorbed on the pre-generated Ag-rich phase, leading to the pt-rich phase formed. After 1 h, as shown in Fig. 4c, the irregular NPs and worm-like structure coexist in the product, and the EDX analysis result suggests that the composition of Pt_xAg_y NPs was 1:1.1 for Ag and Pt elements, approximate equal to the feeding mole ratio of 1:1 for $Pt(NH_3)_4C_2O_4$ and CH_3COOAg, indicating a part of the Ag atoms in Ag-rich phase were diffused into platinum-rich phase. The result further confirms that the worm-like NTs form from the Kirkendall effect with the interdiffusion of two group elements.

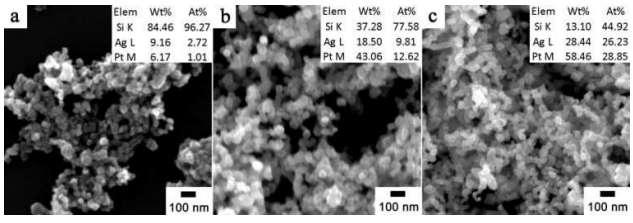

Fig. 4 SEM images and EDX spectrum results (inset images) of $Pt_{52}Ag_{48}$ NTs synthesized under different reaction times: 2 min (a), 4 min (b) and 1 h (c), respectively.

Besides reaction time, the existence of KOH and temperature were also sensitive for the synthesis of the Pt_xAg_y NPs. When no KOH existed or the temperature lower than 160 °C, only CH_3COOAg could be decomposed, and the $Pt(NH_3)_4C_2O_4$ would be gasified out of system instead of reacting. While when the amount of KOH was excessive, the morphology and size of the products have no significant difference. Moreover, when the temperature was increased higher than 170 °C, no worm-like NTs obtained, and only the irregular NPs with the average particle sizes about 81.1±20.1 nm (180 °C) and 73.8±16.6 nm (190 °C) could be observed. (Fig. S4, S5)

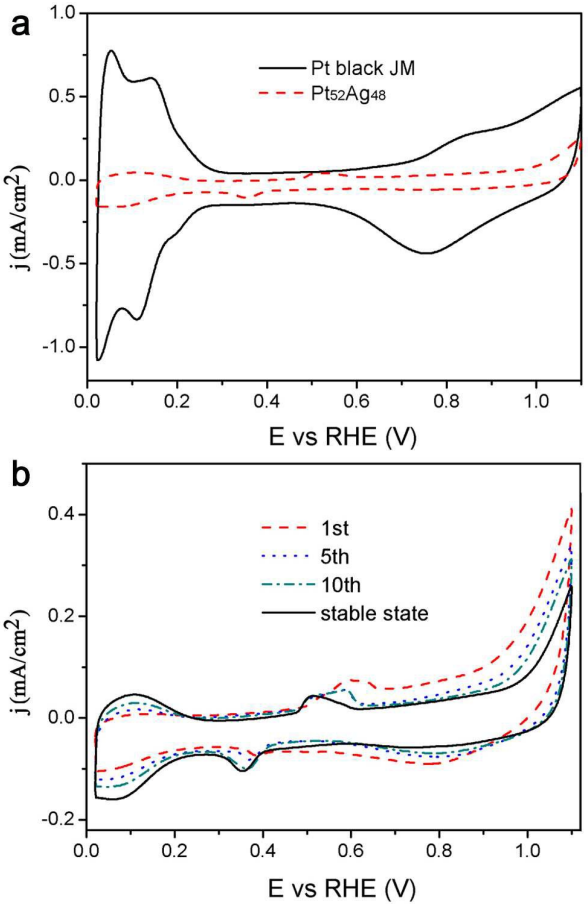

Fig. 5 (a) CV curves of the Pt black (JM) (black solid) and $Pt_{52}Ag_{48}$ (red dash) recorded after 50 cycles in 0.1 M $HClO_4$. (b) Sequential CV curves of the $Pt_{52}Ag_{48}$ catalysts in N_2-saturated 0.1 M $HClO_4$. Scan rate: 50 mV s^{-1}.

Journal Name

ARTICLE

Table 2 The summary of Pt black (JM), $Pt_{11}Ag_{89}$, $Pt_{21}Ag_{79}$, $Pt_{52}Ag_{48}$, $Pt_{79}Ag_{21}$ and $Pt_{86}Ag_{14}$ catalysts for methanol electrooxidation in 0.1M $HClO_4$ + 1M MeOH.

Samples	Onset potentials (V)	Peak potentials (V)	Peak current densities j (mA/cm^2_{Pt})	Current densities (@ 0.85 V) j (mA/cm^2_{Pt})	I_f/I_b
Pt black	0.40	0.95	2.69	1.94	0.99
$Pt_{11}Ag_{89}$	0.38	0.86	0.61	0.61	4.79
$Pt_{21}Ag_{79}$	0.32	0.90	2.71	2.57	1.63
$Pt_{52}Ag_{48}$	0.30	0.84	2.86	2.84	1.72
$Pt_{79}Ag_{21}$	0.30	0.86	1.88	1.87	2.76
$Pt_{86}Ag_{14}$	0.30	0.84	1.16	1.14	1.86

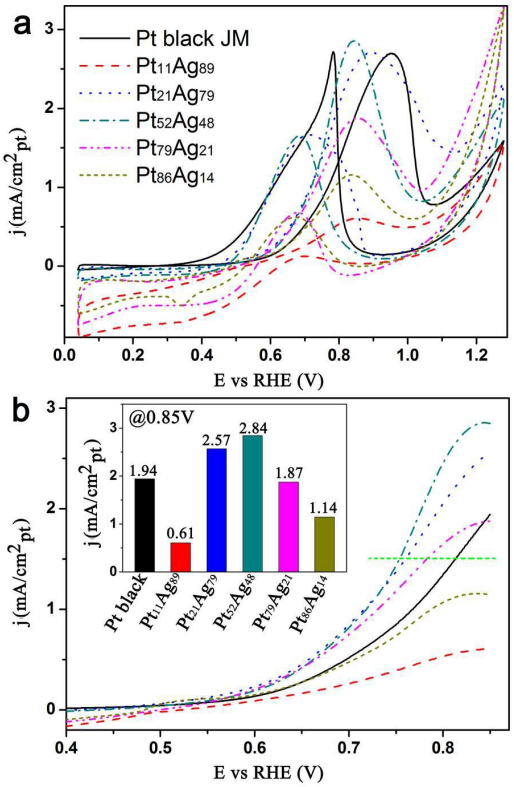

Fig. 6 (a) CV curves and (b) linear sweep voltammetry of Pt black (JM) (black solid), $Pt_{11}Ag_{89}$ (red dash), $Pt_{21}Ag_{79}$ (blue dot), $Pt_{52}Ag_{48}$ (dark cyan dash dot), $Pt_{79}Ag_{21}$ (magenta dash dot dot) and $Pt_{86}Ag_{14}$ (dark yellow short dash) catalysts in 0.1 M $HClO_4$ + 1 M MeOH. Insert image was the histogram of the area current density at 0.85 V (vs. RHE) for Pt black and Pt_xAg_y catalysts. Scan rate: 50 mV s^{-1}.

Electrocatalytic characterization of the Pt_xAg_y NPs catalysts was performed by using cyclic voltammetry methods. The representative CV curves of the $Pt_{52}Ag_{48}$, Pt black (JM) catalysts were shown in Fig. 5a. For commercial Pt black (JM) atalyst, the classic CV features of the Pt catalyst in the acid electrolyte were observed, such as the Hadsorption/ desorption region (0.02-0.3 V), a smooth double layer region (0.3-0.6 V), and the Pt oxides formation and reduction region (positive more than 0.6 V) [27]. While CV curve of the PtAg alloy NPs in the range of 0.02-1.1 V presents a couple of the Ag redox peaks, as well as the H adsorption/ desorption region[28]. The anodic peak was attributed to the oxidative dissolution/ dealloying of Ag from the alloyed PtAg NPs at 0.5-0.6 V, and the cathodic feature at 0.3-0.4 V associated with the reductive deposition/ alloying of Ag into the alloyed PtAg NPs[29-31]. As one can see from Fig. 5b, during the Sequential CV treatment of $Pt_{52}Ag_{48}$ NPs, the Ag atoms were dealloyed from the NPs surface, which led to the development of the more exposed Pt surface and higher electrochemical surface area (ECSA) for the H adsorption/ desorption region (0-0.30 V), due to the exposed Ag surface would be inactive for H adsorption/ desorption[32]. Furthermore, the redox peaks of Ag did not disappear even after 50 cycles, indicating that Ag still exists in the surface layer of the NPs. (Fig. 5b)

Fig. 6a shows the voltammogram of methanol oxidation on the commercial Pt black (JM), $Pt_{11}Ag_{89}$, $Pt_{21}Ag_{79}$, $Pt_{52}Ag_{48}$, $Pt_{79}Ag_{21}$, and $Pt_{86}Ag_{14}$catalysts in the 0.1 M $HClO_4$ + 1 M MeOH solution. The values of the area current density were calculated based on the ECSA (list in table S1), which calculated from the CV data[33]. As summarized in Table 2, the

peak current densities in the forward scan for the methanol oxidation are 2.69, 2.71 and 2.86 mA/cm$^2_{Pt}$ on the Pt black, $Pt_{21}Ag_{79}$ and $Pt_{52}Ag_{48}$ catalysts, respectively. Similarly, the area current densities of the $Pt_{21}Ag_{79}$ and $Pt_{52}Ag_{48}$ catalysts measured at 0.85 V are about 1.3 and 1.5 times higher than that of Pt black (insert image in Fig. 6b), respectively. Furthermore, almost all alloy catalysts present a more negative peak potential, indicating a higher CO_{ads} oxidation activity on alloy catalysts. Especially, the peak potential of $Pt_{52}Ag_{48}$ catalyst reaches to a value of 0.84 V, which shifts negatively by 110 mV from the value of 0.95 V for the Pt black.

The tolerance ability of the catalyst to the accumulation of carbonaceous species can be described by the ratio between the value of forward peak current (I_f) and the backward peak current (I_b) [11, 34]. As shown in Table 2, the I_f/ I_b ratios for Pt black (JM), $Pt_{11}Ag_{89}$, $Pt_{21}Ag_{79}$, $Pt_{52}Ag_{48}$, $Pt_{79}Ag_{21}$, and $Pt_{86}Ag_{14}$ catalysts were 0.99, 4.79, 1.63, 1.72, 2.76 and 1.86, respectively. It suggests that Pt_xAg_y alloy NPs have a better activity in direct oxidation of the carbonaceous accumulated and methanol to carbon dioxide during the process of forward scanning. It has been reported by Feng[35] and He[36] that the properties of anti-poisoning for Pt in acidic electrolytes can be greatly improved with the presence of Ag in the PtAg alloy, and our result further prove that the activity of Pt_xAg_y alloy catalysts toward MOR can be promoted by the process of Ag oxidative dissolution and reductive deposition. To investigate the catalysts performance at low potentials, their onset potentials for MOR are listed in Table 2. Among all the Pt_xAg_y and Pt black catalysts, the $Pt_{52}Ag_{48}$ NPs shows the most negative onset potential and peak potential, which indicates that the $Pt_{52}Ag_{48}$ catalyst has a better catalytic performance toward MOR than that of the Pt black. Fig.7a shows the typical voltammograms of formic acid oxidation on the catalysts of Pt black (JM), $Pt_{11}Ag_{89}$, $Pt_{21}Ag_{79}$, $Pt_{52}Ag_{48}$, $Pt_{79}Ag_{21}$, and $Pt_{86}Ag_{14}$in the 0.1 M $HClO_4$ + 0.5 M HCOOH solution. As listed in Table 3, the first small anodic peak potential and current values in the forward scan were 0.57 V and 2.45 mA/cm$^2_{Pt}$ for $Pt_{11}Ag_{89}$, 0.54 V and 1.04mA/cm$^2_{Pt}$ for $Pt_{21}Ag_{79}$, 0.54 V and 1.78 mA/cm$^2_{Pt}$ for $Pt_{52}Ag_{48}$, 0.50 V and 1.95 mA/cm$^2_{Pt}$ for $Pt_{79}Ag_{21}$ and 0.52 V and 2.84 mA/cm$^2_{Pt}$ for

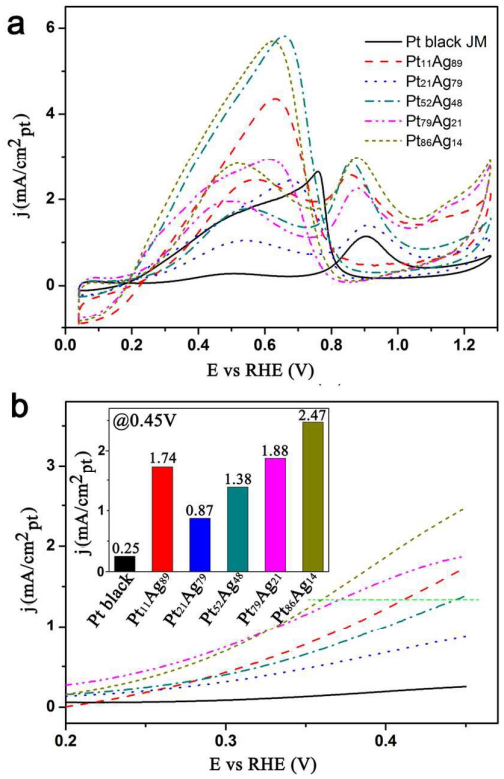

Fig. 7 (a) CVcurves and (b) linear sweep voltammetry of Pt black (JM) (black solid), $Pt_{11}Ag_{89}$ (red dash), $Pt_{21}Ag_{79}$ (blue dot), $Pt_{52}Ag_{48}$ (dark cyan dash dot),$Pt_{79}Ag_{21}$ (magenta dash dot dot) and $Pt_{86}Ag_{14}$ (dark yellow short dash) catalysts in 0.1 M $HClO_4$ + 0.5 M HCOOH. Insert image was the histogram of the area current density at 0.45 V (vs. RHE) for Pt black and Pt_xAg_y catalysts. Scan rate: 100 mV s^{-1}.

Table 3 The summary of Pt black (JM), $Pt_{11}Ag_{89}$, $Pt_{21}Ag_{79}$, $Pt_{52}Ag_{48}$, $Pt_{79}Ag_{21}$ and $Pt_{86}Ag_{14}$ catalysts for formic acid electrooxidation in 0.1M $HClO_4$ + 0.5 M HCOOH.

Samples	Onset potentials (V)	The first peak potentials (V)	The first peak current densities j (mA/cm$^2_{Pt}$)	The second peak potentials (V)	The second peak current densities j (mA/cm$^2_{Pt}$)	Current densities (@ 0.45 V) j (mA/cm$^2_{Pt}$)
Pt black	0.28	0.51	0.28	0.91	1.14	0.25
$Pt_{11}Ag_{89}$	0.16	0.57	2.45	0.86	2.56	1.74
$Pt_{21}Ag_{79}$	0.16	0.54	1.04	0.91	1.39	0.87
$Pt_{52}Ag_{48}$	0.18	0.54	1.78	0.86	2.87	1.38
$Pt_{79}Ag_{21}$	0.15	0.50	1.95	0.88	2.26	1.88
$Pt_{86}Ag_{14}$	0.17	0.52	2.84	0.88	2.98	2.47

Journal Name

ARTICLE

$Pt_{86}Ag_{14}$, respectively. Compared with the corresponding values of 0.51 V and 0.28 mA/cm^2_{Pt} for Pt black (JM), $Pt_{86}Ag_{14}$ catalyst presents a more than 10 times enhancement. Similarly, at 0.45 V, the current value of $Pt_{86}Ag_{14}$ catalyst shows about 9.9 times higher than that of Pt black. (Insert image in Fig. 7b) In addition, the onset potential of the Pt_xAg_y alloy negatively shift about 100-130 mV compared to the Pt black can be observed in the Table 3, indicating that the less accumulation and the more easy oxidation of CO ads on the Pt_xAg_y alloy surface contribute to a large enhancement in durability[37]. And the 100-130 mV negatively shift of the onset potential will lead to about 20%-26% enhancement in electric efficiency, because only less than 0.5 V output voltages can be given by a direct fuel cell under a reasonable current density[38]. Furthermore, as indicated by the dark yellow short dash shown in Fig. 7b, the relevant potential of $Pt_{86}Ag_{14}$ was lower than those of Pt_xAg_y and Pt black at a given oxidation current density values, suggesting that the $Pt_{86}Ag_{14}$ catalyst has a much higher electrochemical catalytic ability for HCOOH.

4. Conclusions

In summary, we have developed a green molten salts approach for the preparation of wormlike Pt_xAg_y alloy NTs without using any organic solvent, surfactant or capping agent. The electrooxidation of $Pt_{52}Ag_{48}$ for methanol and $Pt_{86}Ag_{14}$for formic acid exhibit a much better performance than commercial Pt black catalyst. This green molten salts synthesis method has the potential to be explored to the fabrication of other surfactant or capping agent-free alloys, such as PtPd, PtAu, PtRu, PtRh, etc.

Acknowledgements

This work is supported by National Natural Science Foundation of China (No. 51271135), the program for New Century Excellent Talents in university (No. NCET-12-0455), the Fundamental Research Funds for the Central Universities, the project of Innovative Team of Shaanxi Province (No. 2013KCT-05), the Scientific and Technological Innovation Programs of Higher Education Institutions in Shanxi Province (No. 2015180), and PhD Research Startup Foundation of Shanxi Datong University (No. 2013-B-16).

Notes and references

1 H. You, S. Yang, B. Ding, H. Yang, *Chem. Soc. Rev.*, 2013, **42**, 2880.

2 S. Yang and X. Luo, *Nanoscale*, 2014, **6**, 4438.

3 A. A. Ensafi, M. JafariAsl, B. Rezaei, M. M. Abarghoui and H. Farrokhpour, *J. Power Sources*, 2015, **282**, 452.

4 S. Guo and E. Wang, *Nano Today*, 2011, **6**, 240.

5 Z. Peng, H. You and H. Yang, *ACS nano*, 2010, **4**, 1501.

6 B. J. Hwang, S. M. Senthil Kumar, C.H. Chen, R.W. Chang, D.G. Liu and J.F. Lee, *J. Phys. Chem. C*, 2008, **112**, 2370.

7 Y. Feng, J. Ma, G. Zhang, G. Liu and B. Xu, *Electrochem. Commun.*, 2010, **12**, 1191.

8 H. Yang, L. Dai, D. Xu, J. Fang and S. Zou, *Electrochim. Acta*, 2010, **55**, 8000.

9 Q. Liu, Z. Yan, N. L. Henderson, J. C. Bauer, D. W. Goodman, J. D. Batteas and R. E. Schaak, *J. Am. Chem. Soc.*, 2009, **131**, 5720.

10 M. Gong, G. Fu, Y. Tang, Y. Chen and T. Lu, *ACS Appl. Mater. Interfaces*, 2014, **6**, 7301.

11 S. Yang, Z. Peng and H. Yang, *Adv. Funct. Mater.*, 2008, **18**, 2745.

12 M. Gong, F. Li, Z. Yao, S. Zhang, J. Dong, Y. Chen and Y. Tang, *Nanoscale*, 2015, **7**, 4894.

13 A. Yin, X. Min, Y. Zhang and C. Yan, *J. Am. Chem. Soc.*, 2011, **133**, 3816.

14 Q. Yuan, D. Huang, H. Wang and Z. Zhou, *Langmuir*, 2014, **30**, 5711.

15 J. Wu, J. Zhang, Z. Peng, S. Yang, F. T. Wagner and H. Yang, *J. Am. Chem. Soc.*, 2010, **132**, 4984.

16 B. Lim, M. Jiang, P. H. Camargo, E. C. Cho, J. Tao, X. Lu, Y. Zhu and Y. Xia, *Science*, 2009, **324**, 1302.

17 Y. Song, R. M. Dorin, R. M. Garcia, Y. Jiang, H. Wang, P. Li, Y. Qiu, F. v. Swol, J. E. Miller and J. A. Shelnutt, *J. Am. Chem. Soc.*, 2008, **130**, 12602.

18 M. T. Koper, *Nanoscale*, 2011, **3**, 2054.

19 H. Zhao, J. Wu, H. You, S. Yang, B. Ding, Z. Yang, X. Song and H. Yang, *J. Mater. Chem.*, 2012, **22**, 12046.

20 H. Zhao, S. Yang, H. You, Y. Wu and B. Ding, *Green Chem.*, 2012, **14**, 3197.

21 H. Zhao, C. Yu, H. You, S. Yang, Y. Guo, B. Ding and X. Song, *J. Mater. Chem.*, 2012, **22**, 4780.

22 J. Xu, T. Zhao and Z. Liang, *J. Phys. Chem. C*, 2008, **112**, 17362.

23 Y. Yin, R. M. Rioux, C. K. Erdonmez, S. Hughes, G. A. Somorjai and A. P. Alivisatos, *Science*, 2004, **304**, 711.

24 M. Knez, R. Scholz, K. Nielsch, E. Pippel, D. Hesse, M. Zacharias and U. Gösele, *Nat. Mater.*, 2006, **5**, 627.

25 Z. Peng and H. Yang, *J. Solid State Chem.*, 2008, **181**, 1546.

26 F. N. Rhines, *Phase diagrams in metallurgy: their development and application*, McGraw-Hill Companies, 1956.

27 J. Wu and H. Yang, *Nano Research*, 2011, **4**, 72.

28 Y. Feng, L. Bi, Z. Liu, D. Kong and Z. Yu, *J. Catal.*, 2012, **290**, 18.

29 L. C. Nagle, A. J. Ahern and D. L. Burke, *J. Solid State Electrochem.*, 2002, **6**, 320.

30 B. Jovic, V. Jovic and G. Stafford, *Electrochem. Commun.*, 1999, **1**, 247.

31 F. H. Lima, C. D. Sanches and E. A. Ticianelli, *J. Electrochem. Soc.*, 2005, **152**, 1466.

32 M. Chatenet, M. Aurousseau, R. Durand and F. Andolfatto, *J. Electrochem. Soc.*, 2003, **150**, 47.

33 E. P. Lee, Z. Peng, D. M. Cate, H. Yang, C. T. Campbell and Y. Xia, *J. Am. Chem. Soc.*, 2007, **129**, 10634.

34 R. Mancharan and J. B. Goodenough, *J. Mater. Chem.*, 1992, **2**, 875.

35 L. Feng, G. Gao, P. Huang, X. Wang, C. Zhang, J. Zhang, S. Guo and D. Cui, *Nanoscale Res. Lett.*, 2011, **6**, 1.

36 W. He, X. Wu, J. Liu, K. Zhang, W. Chu, L. Feng, X. Hu, W. Zhou and S. Xie, *Langmuir*, 2009, **26**, 4443.

37 G. Fu, B. Xia, R. Ma, Y. Chen, Y. Tang and J. Lee, *Nano Energy*, 2015, **12**, 824.

38 Z. Yan, J. Xie and P. K. Shen, *J. Power Sources*, 2015, **286**, 239.